PCCP

Accepted Manuscript

ROYAL SOCIETY OF CHEMISTRY

www.rsc.org/pccp

Finite pulse effects in CPMG pulse trains on paramagnetic materials

Michal Leskes and Clare P. Grey*

Department of Chemistry, University of Cambridge, Lensfield Road, CB2 1EW, Cambridge, UK

*cpg27@cam.ac.uk

Abstract

The Carr-Purcell-Meiboom-Gill (CPMG) sequence is commonly used in high resolution NMR spectroscopy and in magnetic resonance imaging for the measurement of transverse relaxation in systems that are subject to diffusion in internal or external gradients and is superior to the Hahn echo measurement, which is more sensitive to diffusion effects. Similarly, it can potentially be used to study dynamic processes in electrode materials for lithium ion batteries. Here we compare the ^{7}Li signal decay curves obtained with the CPMG and Hahn echo sequences under static conditions (i.e., in the absence of magic angle spinning) in paramagnetic materials with varying transition metal ion concentrations. Our results indicate that under CPMG pulse trains the lifetime of the ^{7}Li signal is substantially extended and is correlated with the strength of the electron-nuclear interaction. Numerical simulations and analytical calculations using Floquet theory suggest that the combination of large interactions and a train of finite pulses, results in a spin locking effect which significantly slows the signal's decay. While these effects complicate the interpretation of CPMG-based investigations of diffusion and chemical exchange in paramagnetic materials, they may provide a useful approach to extend the signal's lifetime in these often fast relaxing systems, enabling the use of correlation experiments. Furthermore, these results highlight the importance of developing a deeper understanding of the effects of the large paramagnetic interactions during multiple pulse experiments in order to extend the experimental arsenal available for static and in-situ NMR investigations of paramagnetic materials.

Keywords: paramagnetic NMR, in-situ NMR lithium ion batteries, CPMG, finite pulse effects

1. Introduction

Paramagnetic solids are often challenging to investigate by standard solid-state nuclear magnetic resonance (ssNMR) techniques due to the presence of very large electron-nuclear interactions, often exceeding available magic angle spinning (MAS) frequencies and the excitation bandwidth of radio-frequency pulses. Nevertheless NMR can provide valuable information on the local structure and dynamic processes in these materials, which can then be related to their functionality. As such, NMR spectroscopy has been increasingly used in the study of metalloproteins containing paramagnetic centres[1] as well as inorganic materials containing a much denser network of transition metals, as found, for example, in many electrode materials used for lithium and sodium-ion batteries[2].

NMR studies of battery electrode materials are most commonly performed ex-situ by extracting the electrode material (typically a transition metal oxide or phosphate) from the battery cell at different states of charge. The resonance frequency of the nuclei that are coupled to the unpaired electrons in the paramagnetic centres is shifted by the through-bond Fermi contact interaction and the spectra are broadened by the through-space dipolar interaction (which can also cause additional shifts). These measurements benefit from very fast MAS, which often results in sufficient resolution, especially when combined with two dimensional techniques for separating the large side band manifolds from the isotropic resonances[3–5]. The resolved resonances can then be assigned to local environments in the material, corresponding to different transition metal coordination shells surrounding the detected nucleus. However, in order to capture transient species and study electrochemical processes in real time, NMR must be performed in-situ, in parallel with the battery's operation[6]. In this case, the measurement is, to date, performed on static samples, due to the challenges associated with spinning metal and the liquid and semi-solid components. This results in poor resolution of the isotropic resonances, especially in the presence of the strong anisotropic dipolar interactions characteristic of paramagnetic materials and bulk magnetic susceptibility (BMS) effects[7]. Significant information can still be gained on relevant processes such as diffusion, chemical exchange and phase transformations by following changes in other NMR properties such as the spin-lattice (T_1) and spin-spin (T_2) relaxation and peak width while charging and discharging the battery.

This approach has been recently demonstrated on the spinel cathode material, $Li_{1.08}Mn_{1.92}O_4$[7,8]. In this case, the transverse relaxation decay constants were shown to be good probes of processes such as exchange within the cathode material and were also used to identify order-disorder phase transformations upon lithium removal. These measurements were performed using the Hahn echo sequence, employing a single echo pulse with a variable echo delay. However, echo measurements are known to be sensitive to diffusional processes, which will contribute to the measured decay curve (defined by the constant T_2') in addition to the T_2 relaxation. Such processes are expected to occur in operating battery cells in which the detected species (such as Li^+) diffuse through the particles of the electrochemically active material, into the electrolyte, via a composite electrode structure. Thus strong internal magnetic field gradients due to the variation in magnetic susceptibility in the path of the diffusing nuclei are expected to affect the measurement.

The Carr-Purcell-Meiboom-Gill (CPMG) sequence[9,10] offers an alternative approach for measuring transverse relaxation rates, often used in liquid state NMR and magnetic resonance imaging (MRI) since it can reduce or eliminate the effect of diffusion on the measured decay curves. Moreover, by varying the inter-pulse delay in the CPMG pulse train one can obtain insight into the time scale and nature of dynamic processes in the sample. This approach was used to probe decoherence effects for developing improved dynamical decoupling schemes in quantum information processing[11]. Furthermore, varying the CPMG echo delays, while keeping the overall signal decay time constant can be used to characterize exchange processes[12,13] and diffusion in restricted spaces[14]. Similarly it can be expected that CPMG sequences can be applied to paramagnetic electrode materials where some dynamic processes are taking place to either measure decay constants closer to the internal transverse relaxation or to investigate the nature of the dynamics.

Here we compare the performance of these two approaches, Hahn echo and CPMG, for measuring transverse relaxation (in static samples) in two series of mixed olivine materials of composition $LiM_xMg_{1-x}PO_4$ with M=Mn(II) or Fe(II) as a function of x. These series, with varying extent of paramagnetic-ion substitution, allow us to evaluate the effect of increasing the anisotropic interactions on the measured decay curves using both Hahn echo and CPMG sequences. MAS spectra were also acquired to characterise the anisotropic interactions. The differences in T_2' constants obtained with the two sequences for compositions with high paramagnetic ions content are accounted for by numerical simulations on a simple model system, without including relaxation or exchange effects. Derivation of the effective Hamiltonian governing the signal evolution during the CPMG pulse train using the Floquet formalism[15] shows that finite pulses play a significant role in controlling the CPMG performance, resulting in long-lived signals, especially in the presence of large anisotropic interactions.

Finite pulse effects were shown to result in long lived signals during CPMG in diamagnetic materials such as C_{60}, Y_2O_3 and doped Si[16–18]. Several possible explanations have been discussed in the literature for long lived spin echoes in dipolar solids. The Barrett et al. analysis was based on average Hamiltonian theory (AHT) and numerical simulations showing that the effect is mostly due to many-body dipolar interactions.[17,19] By contrast, Levstein et al. attributed these effects to pulse errors resulting in stimulated echo contributions and T_1 effects[18,20]. Recent work by Walls et al. addressed the case of long echo delays in the CPMG train, their AHT analysis showing that inclusion of dipolar couplings during the finite pulses did not contribute significantly to the spin lock effect observed in simulations and experiments[21]. Here we analyse the limit of very large interactions (up to two orders of magnitude larger than the interactions present in the diamagnetic systems) with relatively long echo delays in the CPMG pulse train with high power pulses. The use of Floquet theory is advantageous in this case as it provides an exact form of the time independent Hamiltonian, which can then be diagonalized providing insight into the performance of the CPMG sequence.

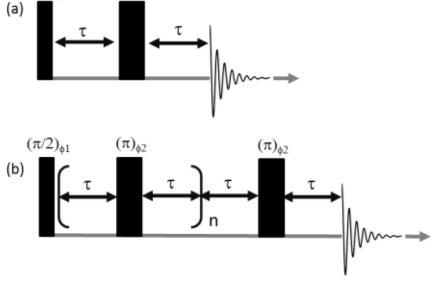

Figure 1 Pulse sequences used for measuring transverse signal decay: (a) Hahn echo with ϕ1 = x,y,-x,-y; ϕ2 = x,x,x,x,y,y,y,y,-x,-x,-x,-x,-y,-y,-y,-y; $\phi_{receiver}$ = x,-y,-x,y,-x,y,x,-y, signal was measured as a function of τ. (b) CPMG with ϕ1 = x,x,-x,-x,y,y,-y,-y; ϕ2 = y,-y,y,-y,x,-x,x,-x; $\phi_{receiver}$ = x,x,-x, -x,y,y,-y,-y; the signal was measured as a function of the number of echo blocks, n, with fixed τ. The basic period of the CPMG sequence, forming a cyclic unit, is given by $\tau_c = 4\tau + 2\tau_p$, with τ_p the length of the π pulse. In both cases, the last echo delay accommodates the probe dead time.

2. Experimental techniques

^{7}Li NMR experiments were performed on a 4.7 T Bruker 200 AVANCEIII spectrometer using an Ago Samoson 1.8 mm probe. The Hahn echo and CPMG pulse sequences (provided by Bruker and operating within the TOPSPIN software (Figure 1)) were used to measure the magnetization decay in a pseudo 2D manner: the signal was recorded and Fourier transformed following evolution in the indirect dimension, which consisted of either an echo pulse with varying echo delay, τ, or an increasing number echo pulses, n, with fixed echo delay in the Hahn echo and CPMG experiments, respectively. The echo delays varied in the range of 10-1200 µs in the Hahn echo experiments and were set to 8.5 µs for CPMG (unless stated otherwise). Experiments were performed on static samples using a (^{7}Li) RF amplitude of 167 kHz (π pulse of 3 µs) and a relaxation delay that was optimized for each sample. The static powder pattern was integrated for all increments and the integrated intensity was plotted as a function of time in the indirect dimension. The number of scans, the echo delay τ in the Hahn echo sequence and the number of echoes n in the CPMG train, were optimised for each sample. The number of scans was kept constant in the Hahn echo and CPMG measurements for the same sample. MAS measurements were performed at 35 kHz and the spinning side band manifold was fitted using the TOPSPIN software.

$LiMn_xMg_{1-x}PO_4$ and $LiFe_xMg_{1-x}PO_4$ samples were synthesized following standard solid state synthesis route as discussed in prior publications[22].

3. Results and Discussion

3.1. Experiments

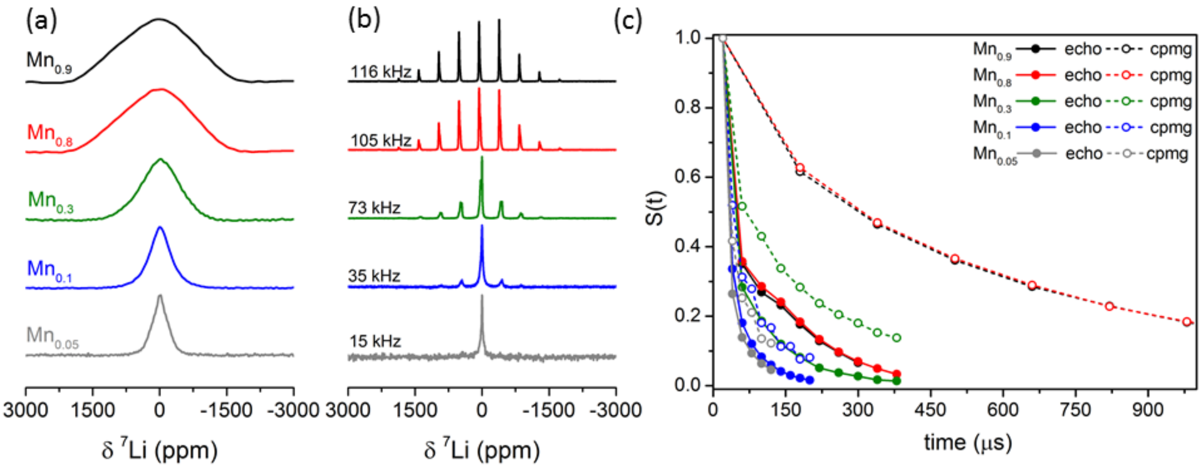

Figure 2 (a) Static ^{7}Li solid echo NMR spectra of the series $LiMn_xMg_{1-x}PO_4$, where the Mn content is specified on the LHS. (b) ^{7}Li MAS spectra acquired at 35 kHz with the corresponding approximated electron-nuclear dipolar coupling anisotropy (fitted by treating this as a CSA) specified on the LHS (when several environment are resolved as for $Mn_{0.3}$, $Mn_{0.8}$ and $Mn_{0.9}$ compositions the anisotropy of the major component is specified) . (c) ^{7}Li signal decay curves obtained by integrating the static line shapes obtained using either a Hahn echo (full circles) or CPMG (open circles) sequence.

The static ^{7}Li NMR spectra of the series $LiMn_xMg_{1-x}PO_4$ are plotted in Figure 2a. The main interactions contributing to the spectral broadening are the electron-nuclear (e-n) dipolar couplings, the quadrupolar interaction and the ^{7}Li homonuclear dipolar couplings. The ^{7}Li resonance broadens with

Compound	**Hahn echo T_2' in μs**	**CPMG T_2' in μs**
$LiMn_{0.05}Mg_{0.95}PO_4$	13(1)	19(2)
$LiMn_{0.1}Mg_{0.9}PO_4$	19(2)	30(3)
$LiMn_{0.3}Mg_{0.7}PO_4$	33(8)	65(10)
$LiMn_{0.8}Mg_{0.2}PO_4$	44(8)	413(31)
$LiMn_{0.9}Mg_{0.1}PO_4$	35(7)	402(33)
$LiFe_{0.1}Mg_{0.9}PO_4$	84(6)	590(60)
$LiFe_{0.8}Mg_{0.2}PO_4$	154(20)	770(50)
$LiFe_{0.9}Mg_{0.1}PO_4$	86(12)	595(50)
$LiFePO_4$	98(5)	800(40)

Table 1 T_2' constants (error in brackets) determined by a mono-exponential fit to the decay curves in Figure 2c and 3c.

increasing Mn concentration and, as the quadrupolar and homonuclear couplings are independent of the Mn/Mg ratio (assuming there is no significant change in the structure caused by cation substitution[23,24]), it is likely that the e-n interactions are the cause for the increased broadening. The unpaired electrons on the $3d^5$ high spin Mn(II) ions couple to the ^{7}Li nuclei, however, due to the fast electronic relaxation time (compared with the time scale of the NMR measurement), the nuclear spins couple with the time-averaged magnetic moment of the electrons. In contrast to the dipolar coupling tensor, the e-n dipolar couplings resemble the chemical shielding anisotropy (CSA) interaction and produce similar powder patterns. Coupling to a single electron results in an axially symmetric tensor while couplings to multiple electrons are additive, resulting in symmetry which depends on the geometry around the nuclear site[25,26]. Thus in the following we will refer to the e-n coupling simply as the CSA and the results should be applicable to both cases (CSA and e-n dipolar tensors). Since ^{7}Li is a spin 3/2 nucleus, the CSA interaction will broaden all three transitions, the central and satellite transitions, the latter also being broadened by the 1st order quadrupolar interaction. The ^{7}Li homonuclear dipolar couplings result in additional, smaller broadening.

The extent of the anisotropy as a function of Mn concentration was evaluated by fitting the ^{7}Li MAS sideband manifolds (Figure 2b). For all the fits the quadrupolar parameters were kept constant with a coupling constant $|Cq| = 60$ kHz and asymmetry $\eta=1.0$. These values are an approximation determined by comparing the ^{6}Li and ^{7}Li spectra of $LiFePO_4$ (see Figure S1 in supporting information). While the exact quadrupole parameters may slightly vary for $LiMnPO_4$, only small changes in the C_q, of the order of 5-10 kHz, are expected within a series based on ab-initio calculations[27], thus they will not have a significant effect on the fit. The homonuclear contribution was neglected (as the ^{7}Li couplings are much smaller than the MAS frequency). The approximated CSA values (defined as δ_{zz}-δ_{iso}, where δ_{zz} is the principal component with the largest frequency separation from the isotropic shift given by δ_{iso}) vary between 15 – 116 kHz (Figure 2b, labels on the LHS) as the Mn stoichiometry increases from x= 0.05 to 0.9. This increase is expected as more ^{7}Li nuclei in the material are coupled to a larger number of Mn ions. Since the substitution of Mn by Mg results in a solid solution (a random distribution of the cations on the crystallographic sites)[23,24] there can, in principle, be up to 27 different Li environments (configurations of Mn and Mg around the Li site)[3,5]. However, since the Fermi-contact shifts in these materials are very small (primarily because of the high covalency of the P-O bonds in the olivine structure and thus the high ionicity of the Li-O bonds, which results in only a small transfer of spin density[5,28]) these different environments in most cases do not result in resolvable distinct resonances in the MAS spectra. They do, however, have an inhomogeneous contribution to the width of the centre and spinning sidebands. Some fine structure is observed for the $Mn_{0.3}$ and $Mn_{0.8}$ stoichiometries, the assignment of which is beyond the scope of this study. Note that a very different situation is observed in the ^{31}P spectra of these materials and related solid solutions where a whole series of resonances can be observed corresponding to different local Fe/Mn and Fe/Co configurations[3,5].

The magnetization decay curves of the various phases were measured using the Hahn echo and CPMG sequences (Figure 2c) with high RF amplitudes (larger than or of the order of the CSA interactions). The corresponding T_2' constants, approximated by a mono-exponential fit of the decay curves, are given in Table 1. Considering first the curves measured with Hahn echo (full circles and lines), the signal decays more slowly with increasing concentration of the paramagnetic ions, and thus the T_2' decay constant becomes longer. This phenomenological constant depends on the inherent T_2 relaxation, the homogeneous part of the spin interactions (i.e., the part that is not refocused by the π pulses)[29], and can also be affected by any ionic motion on the μs time scale. The homogeneous part of the spin interactions generally becomes larger with Mn concentration due to the increasing number of e-n dipolar couplings (unless the geometry leads to either complete or partial cancellation of these additive interactions (see later)). The ionic motion is not expected to vary much across the series (although substitution with Mg was shown to improve the kinetic performance of $LiMn_xMg_{1-x}PO_4$ during delithiation[24]). Thus these results indicate that the nuclear transverse relaxation rate decreases with increasing Mn concentration. It is reasonable to assume that a major source of nuclear relaxation is the coupling to the electrons. Thus the slower rate observed with increased concentration of paramagnetic centres is likely a result of increased exchange interactions and shorter electron relaxation times, shifting the spectral density to higher frequency and consequently – resulting in lower spectral density in the MHz frequency range.

A similar phenomenon is observed with the CPMG pulse trains, resulting in longer T_2' constants with increasing Mn concentration. Furthermore the deviation between the decay curves obtained with CPMG compared with those of the Hahn echo increases with Mn concentration. This effect could be due to the decreased sensitivity of the CPMG sequence to ionic motion but again it is unlikely that the motion would increase with Mn concentration. Since this effect is correlated with the magnitude of the anisotropy, it appears, at least in part, to be a coherent effect; this will be discussed further in the following sections.

A similar comparison was performed for a second olivine series, $LiFe_xMg_{1-x}PO_4$. In this case the static pattern and MAS sideband manifolds (Figure 3) are broadest for the $Fe_{0.8}$ stoichiometry (of all the

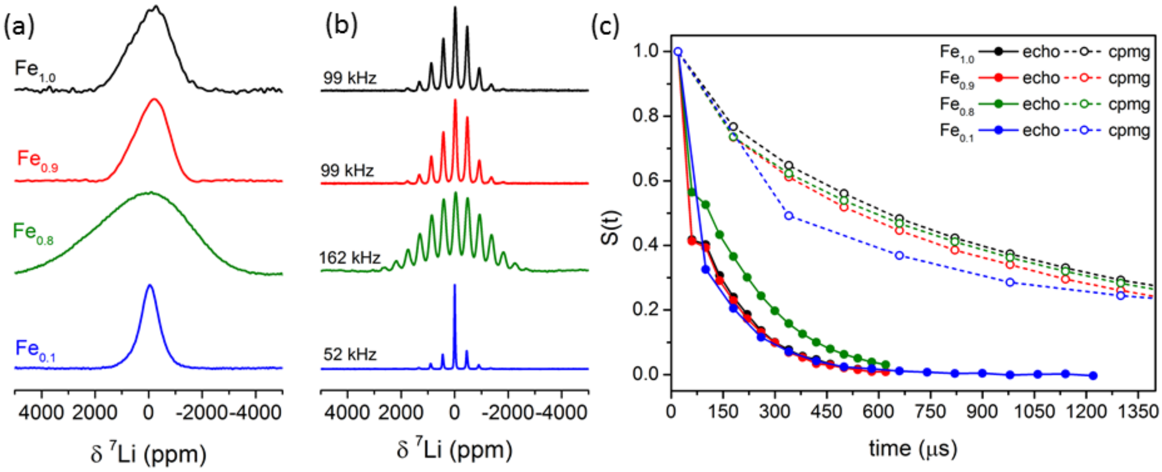

Figure 3 (a) Static ^{7}Li solid echo NMR spectra of the series $LiFe_xMg_{1-x}PO_4$, where the Fe content is specified on the LHS. (b) ^{7}Li MAS spectra acquired at 35 kHz with the corresponding electron-nuclear dipolar coupling anisotropy (fitted as a CSA) specified on the LHS. (c) ^{7}Li signal decay curves obtained by integrating the static line shape using the Hahn echo sequence (full circles) or CPMG (open circles).

samples studied here) and become narrower with increasing Fe content. As discussed above, the smaller broadening in $Fe_{1.0}$ is ascribed to partial cancellation of the dipolar coupling for when the Li ions are surrounded by Fe ions only. This non-linear dependence on the Fe content can be a result of bulk magnetic susceptibility broadening which can display maxima at intermediate concentrations for similar reasons[7,30,31]. Furthermore, additional contributions to the spectral broadening is expected due to the anisotropic susceptibility of Fe(II) which has $3d^6$ high spin electronic configuration (unlike the Mn(II) configuration which has an isotropic d^5 (A_{1g}) state) [32].

The Hahn echo decay curves overlap except for the $Fe_{0.8}$ sample which has a slightly longer T_2'. When CPMG is used, all four compounds display a slower decay than that measured with a Hahn echo, with a slightly slower decay for the compounds with larger anisotropy. Here again the differences between the Hahn echo and the CPMG measurements can be a result of the effect of the large spin interactions as will be explored in the following sections by employing numerical simulations and analysis using Floquet theory.

3.2. Simulations

The performance of the two sequences was compared by numerical simulations using SPINEVOLUTION program[33]. For simplicity a spin system composed of four spin ½ nuclei was considered taking into account homonuclear couplings and CSA interactions for all spins. The four spins were placed at the vertices of a square at an equal distance, R, from the (0,0,0) centre of a Cartesian coordinate system. This geometry was chosen out of convenience as it allowed the effect of the homonuclear dipolar interactions between the spins to be explored by varying a single parameter, R.

Although our experimental results are for a quadrupolar nucleus, due to the small quadupolar coupling of ^{7}Li (about 60 kHz in the olivine phase) it is reasonable to neglect its effect on the central transition. Furthermore, the satellite transitions which are broadened by the 1st order quadrupolar interaction will quickly de-phase (as the 1st order interaction is not refocused by π pulses) and will not contribute significantly to the measured decay curve. A comparison of the decay of the satellite and central transitions using the Hahn echo sequence is given in the supporting information (Figure S2) showing the quick decay of the satellite transitions (to zero within a 10 μs echo delay), even when no CSA is included in the simulation, as compared to the much slower decay of the central transition. Thus modelling the system as spin ½ nuclei is a reasonable approximation.

Signal decay curves were obtained by calculating the observable, $S(t)=\langle I_+\rangle(t)$, for all spins as a function of the echo delay in the Hahn echo or the number of CPMG pulses (with a fixed echo delay) using the phase cycle used in the experiments (caption to Figure 1). The sequences were compared for ideal delta pulses as well as finite pulses with an RF amplitude of 167 kHz. We note that we only consider here the case of relatively high RF amplitudes and exact 180 pulses. The signals were simulated as a function of the CSA (equal for all spins) and the homonuclear interactions without adding relaxation effects. The magnitude of the CSA interaction is given by ω_a and in the case of the electron – nuclear interactions $\omega_a = (\frac{\mu_0}{4\pi})\frac{\mu_B^2 S(S+1)}{3k_B T} g^2 \gamma B_0$, assuming the nuclei are coupled to the time averaged magnetic moment of the electrons, where μ_0 denotes the permeability, μ_B is the Bohr magneton, S the electron spin quantum number, k_B Boltzmann's constant, g the electron g tensor, B_0 the external magnetic field and γ the nuclear gyromagnetic ratio. For simplicity the g-tensor is assumed to be isotropic, as in the case of the Mn (d^5) olivine system. The homonuclear dipolar coupling strength is given by $\omega_{ab} = \sqrt{6}\frac{\mu_0\gamma^2 h}{4\pi r_{ab}^3}$ where r_{ab} is the inter-nuclear distance. The couplings between the four spins were varied by changing their distance, R, from the origin resulting in two couplings strengths for $r_{ab} = 2\text{R}$ and $\sqrt{2}R$. The value obtained when the signal reached a steady state is plotted in Figure 4 as a function of the CSA magnitude, ω_a, and the average of the homonuclear dipolar interactions.

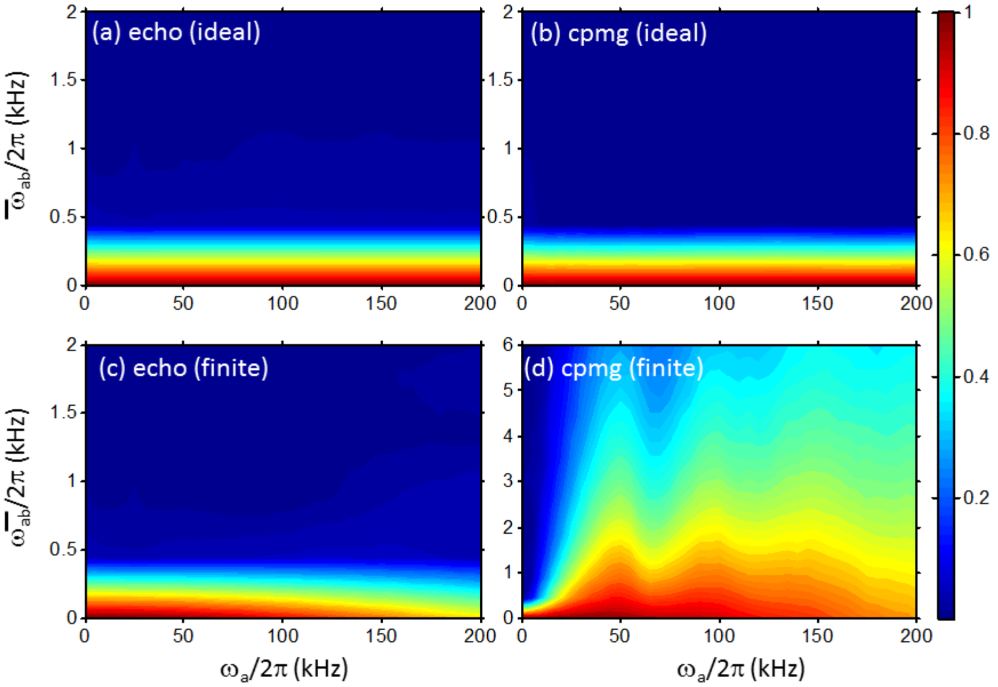

Figure 4 Plot showing the residual signal when it reached a plateau, obtained from a simulation of a system of four (spin ½) nuclei, under the effect of (a,c) a Hahn echo sequence and (b,d) CPMG with (a,b) ideal pulses and (c,d) non-ideal pulses with an RF amplitude equal to 167 kHz. The colour bar on the right indicates the signal intensity with a full signal given by S(0)=1. The Hahn echo calculation was performed by incrementing the echo delay in steps of 10 μs while the CPMG calculation was performed with a delay τ=8.5μs (such that the CPMG cycle time τ_c= 40μs). The calculation was performed as a function of the dipolar coupling and the CSA, which was equal for all spins (with η=1.0). Powder averaging was obtained using the ZCW set[40] with 987 orientations.

As expected when no homonuclear couplings are present, (i.e., ω_{ab}=0), and when using ideal π pulses (Figure 4a-b), the CSA interaction is fully refocused and both Hahn echo and CPMG sequences result in full signal retention (S(t) is close to S(0), red region at the bottom of the plots) . Once these couplings are included in the simulations, since they are not affected by the ideal pulses, they result in complete signal decay even for very weak dipolar interactions. When finite pulses are used the result is very different for the Hahn echo vs. the CPMG (Figure 4c-d) sequence: without homonuclear couplings, in the Hahn echo case, the signal is refocused but for a limited range of CSA. Once the CSA interaction exceeds 20 kHz (for an RF power of 167 kHz) the signal starts to de-phase and about 30% of the signal is lost when the CSA reaches 200 kHz. The CPMG sequence is slightly more efficient in refocusing the signal, resulting in about 25% signal loss for the largest CSA. Significant differences between the two sequences are observed once homonuclear couplings are introduced. While the Hahn echo results in complete signal dephasing when the couplings exceed 400 Hz, the

CPMG sequence results in efficient signal retention even when the couplings are larger than 1 kHz. This effect becomes more significant as the CSA interaction increases.

The closest-neighbour, and therefore strongest, ^{7}Li homonuclear dipolar couplings in the olivine materials vary between 200 Hz (shortest distance between Li in adjacent channels in the olivine structure) and 650 Hz (closest Li within the same channel). Several calculated CPMG signal decay curves are plotted in Figure 5a for an average coupling of 400 Hz between pairs within the 4 spins (for R = 4.2Å), and compared to the decay without dipolar coupling. Slices taken through the contour plots at average dipolar couplings of 400 Hz as well as 0 Hz are shown in Figure 5b as a function of CSA. These two plots show the increase in signal retention achieved with large anisotropies in the presence of homonuclear dipolar interactions. Note that with the phase cycle used here for the CPMG sequence, some contribution to the signal's evolution could, in principle, arise from pathways involving zero quantum coherences via the formation of stimulated echoes[20,34]. These pathways can result in slower decay rates since they depend on the spin-lattice relaxation T_1 (which is larger than T_2 in solids). Such effects were reported when CPMG is used for sensitivity enhancement and were suppressed by a 16-step phase cycle and careful setting of the echo delay[35,36]. However, simulations performed with this 16-step phase cycle did not show significant difference from the performance observed in Figure 5. Furthermore, monitoring the evolution of the different density matrix elements during the train of CPMG pulses did not show significant contribution from pathways involving zero quantum coherences (see Supporting Information for further discussion).

Thus, the numerical simulations clearly indicate that our experimental observations are, at least in part, due to the effect of finite pulses in the presence of very large anisotropic interactions and homonuclear couplings. Further insight can be obtained by derivation of the CPMG effective Hamiltonian as will be discussed in the following section.

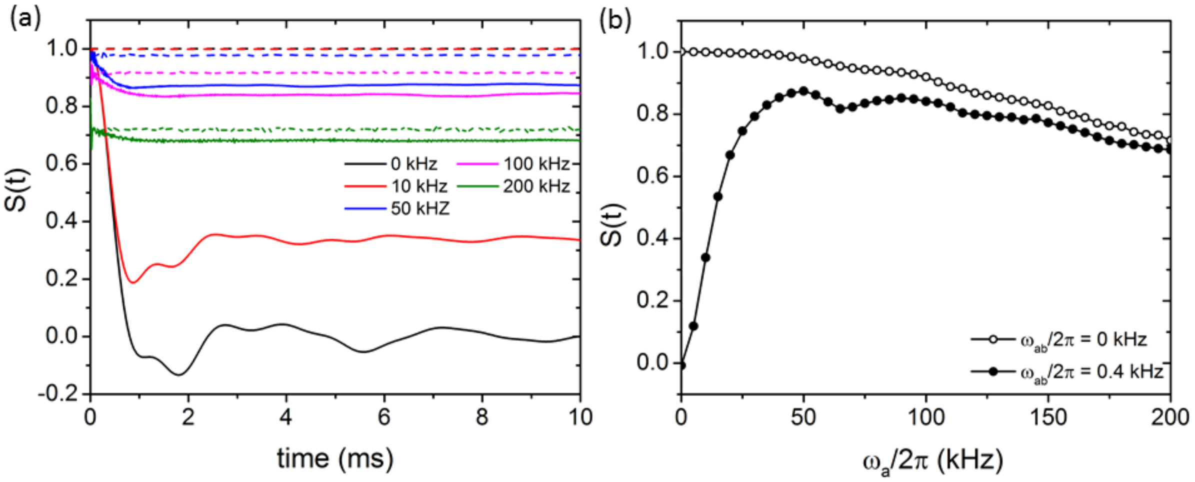

Figure 5 (a) The simulated CPMG decay curves for a system of four (spin ½) nuclei with average dipolar couplings of 0.4 kHz and varying CSA values (full lines) and with no dipolar couplings (dashed lines); in both cases an RF amplitude of 167 kHz was used.(b) Slices taken through the contour plot in figure 4d at dipolar coupling of 0.4 kHz (full circles) and 0 kHz (open circles).

3.3. Theory

To gain insight into the evolution of the spin system under the effect of the train of CPMG pulses let us consider the rotating frame Hamiltonian of a static system of coupled spin-½ nuclei:

$$H(t) = \sum_{a} \omega_a G_a T_{0,a}^{(1)} + \sum_{a>b} \omega_{ab} G_{ab} T_{0,ab}^{(2)} + H^{RF}(t) \quad (1)$$

Here the $T_m^{(l)}$ are the irreducible tensor operators. The first term is the through-space electron-nuclear dipolar interaction represented here as the CSA interaction (due to the fast electron relaxation on the NMR time scale). The G_a coefficients contain the geometric dependence of the CSA tensor and can be calculated by summing the different e-n dipolar tensors (which depend on the electron-nuclear distance) defined in a common frame of reference, diagonalizing the resulting tensor and transforming it to the lab frame defined by the external magnetic field[25]. The second term is the homonuclear dipolar interaction with an orientation dependence factor given by G_{ab}. The isotropic and anisotropic *chemical* shifts of the nuclei are assumed to be much smaller than the "CSA" terms due to the coupling to the electrons and are therefore neglected here. The third term describes the time dependent RF irradiation and is given by:

$$H^{RF}(t) = \omega_1 \left\{ \varepsilon_1(t) T_1^{(1)} + \varepsilon_{-1}(t) T_{-1}^{(1)} \right\} \quad (2)$$

In the case of the CPMG sequence, this describes a periodic train of π pulses of length τ_p separated by a fixed delay τ. The ε coefficients are time dependent due to the discontinuous RF train and are equal to $i\sqrt{2}/2$ (in the case of RF irradiation along the y axis) during the pulse and to zero during the delays. The CPMG sequence is cyclic with a period given by $\tau_c = 4\tau + 2\tau_p$ and in order to evaluate the effect of the repeating RF irradiation on the various interactions, the rotating frame Hamiltonian is transformed to the RF interaction frame using $U^{RF}(t) = \hat{T} e^{-i\int_0^{\tau_c} H^{RF}(t')dt'}$ and

$$H^{int}(t) = U^{RF^{-1}}(t)\{H(t) - H^{RF}(t)\}U^{RF}(t) \quad (3)$$

with $\hat{T}$ the Dyson time ordering operator, resulting in:

$$H^{int}(t) = \sum_{a,m} \omega_a G_a d_m^{(1)}(t) T_{m,a}^{(1)} + \sum_{a>b,m} \omega_{ab} G_{ab} d_m^{(2)}(t) T_{m,ab}^{(2)}. \quad (4)$$

Here the time dependent coefficients $d_m^{(l)}(t)$, are derived by calculating:

$$U^{RF^{-1}}(t) T_0^{(l)} U^{RF}(t) = \sum_m d_m^{(l)}(t)\, T_m^{(l)} \quad (5)$$

and they depend on the values of the RF parameters such as the pulse length, RF amplitude and inter-pulse delay τ_p, ω_1 and τ respectively. These coefficients are plotted in Figure 6 demonstrating that for ideal pulses (delta pulses) only $d_0^{(l)}(t)$ need to be considered while in the case of finite pulses other terms become significant.

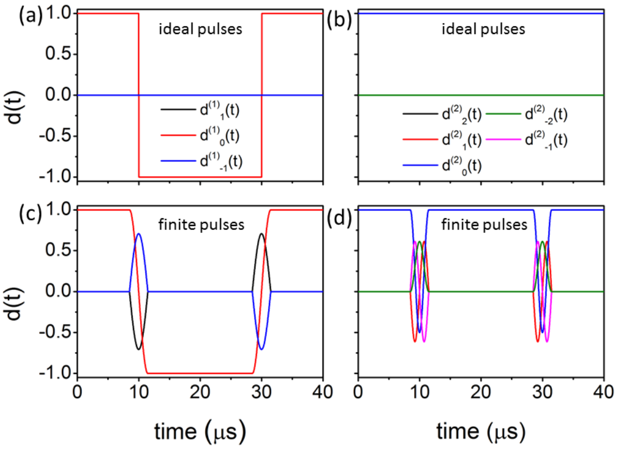

Figure 6 The (a, c) $d^{(1)}_m(t)$ and (b,d) $d^{(2)}_m(t)$ coefficients calculated for a CPMG sequence using (a,b) ideal pulses and τ=10μs and (c,d) non-ideal pulses with length 3μs and τ=8.5μs.

To evaluate the contribution of the different interactions it is convenient to transform the Hamiltonian to a frame where it is time independent and derive an effective Hamiltonian which will allow us to identify the main interactions dominating the spin system evolution during the train of CPMG pulses. Here we employ Floquet theory since it provides an exact form for the time independent Hamiltonian which can then be used to derive the effective Hamiltonian as well as perform an exact calculation of the eigenvalues in the presence of very large interactions[15,37]. The Floquet (time independent) Hamiltonian is given by:

$$\begin{gathered} H_F = \sum_k H_k F_k + \omega_c N \\ H_k = \sum_{a,m} \omega_a G_a d^{(1)}_{m,k} T^{(1)}_{m,a} + \sum_{a>b,m} \omega_{ab} G_{ab} d^{(2)}_{m,k} T^{(2)}_{m,ab}. \end{gathered} \qquad (6)$$

This result is obtained by first expanding the time dependent coefficients in a Fourier series:

$$d^{(l)}_m(t) = \sum_k d^{(l)}_{m,k} e^{ik\omega_c t} \qquad (7)$$

with $\omega_c = 2\pi/\tau_c$, the characteristic frequency of the Hamiltonian, and expressing the Hamiltonian in Fourier space using the ladder operator F_k followed by a transformation to the Floquet representation using the number operator N as described in ref [15].

The matrix form of the Floquet Hamiltonian in Eq. 6 makes it useful in evaluating which terms can become significant: terms which were time dependent due to the CPMG pulses occupy off diagonal blocks with $k \neq 0$ while terms which are not affected by the pulses are on the diagonal with $k = 0$. In the case of finite π pulses the $d^{(l)}_{m,k}$ follow:

$$\begin{gathered} d^{(1)}_{m,k} \neq 0 \; for\; odd\; k \\ d^{(1)}_{0,k} = d^{(1)}_{0,-k} \; and\; d^{(1)}_{1,k} = d^{(1)}_{-1,-k} \\ d^{(2)}_{m,k} \neq 0 \; for\; even\; k \; (m = 0, \mp 1, \mp 2) \; and\; k = 0 \; (m = 0). \end{gathered} \qquad (8)$$

As expected the π pulses modulate the CSA interactions such that their average over an RF period is zero while a significant part of the homonuclear dipolar interactions is unaffected by the π pulses.

Since the e-n couplings in the materials studies here can be as high as 2000 ppm (about 160 kHz at 4.7 T and ^{7}Li Larmor frequency of 77 MHz) they can become significant (when compared to the characteristic frequency ω$_c$) and therefore cannot be neglected even though they are off-diagonal in the Floquet Hamiltonian. To evaluate their effect we first block diagonalize the Floquet Hamiltonian using the van-Vleck transformation[15]. The effective Hamiltonian is then given by the diagonal blocks of the transformed Hamiltonian which to first order are given by:

$$
\begin{aligned}
H^{(0)} &= \sum_{a>b} \omega_{ab} G_{ab} d^{(2)}_{0,0} T^{(2)}_{0,ab} \\
H^{(1)} &= -\sum_{\substack{a,b<c,m,m' \\ k>0}} \omega_{ab} G_{ab} \omega_{bc} G_{bc} \frac{d^{(2)}_{m,k} d^{(2)}_{m',-k}}{k\omega_c} \left[T^{(2)}_{m,ab}, T^{(2)}_{m',bc}\right] \\
&\quad + \sum_{a,k>0} \frac{2(\omega_a G_a)^2}{k\omega_c} d^{(1)}_{0,k} d^{(1)}_{1,k} \left\{T^{(1)}_{1,a} + T^{(1)}_{-1,a}\right\}
\end{aligned}
\qquad (9)
$$

The first term is the residual homonuclear dipolar interaction scaled by $d^{(2)}_{0,0}$ due to the RF pulses. This term will result in signal dephasing during the CPMG pulse train. The first order term has two contributions: the first part is a cross term between the different components of the dipolar interaction and since its operator part is tri-linear it can only contribute further to signal dephasing (this term is however much smaller than the zero-order effective Hamiltonian, $H^{(0)}$). The second part is a cross term of the CSA interaction formed due to the finite length of the pulses and is proportional to the square of the interaction scaled by 1/ω$_c$. The spin part of this term is a linear operator proportional to $I_{y,a}$ for all spins. This term is the most significant in the Hamiltonian and it dominates the spin system evolution during the CPMG pulses. Its well-defined direction (determined by the direction of the π

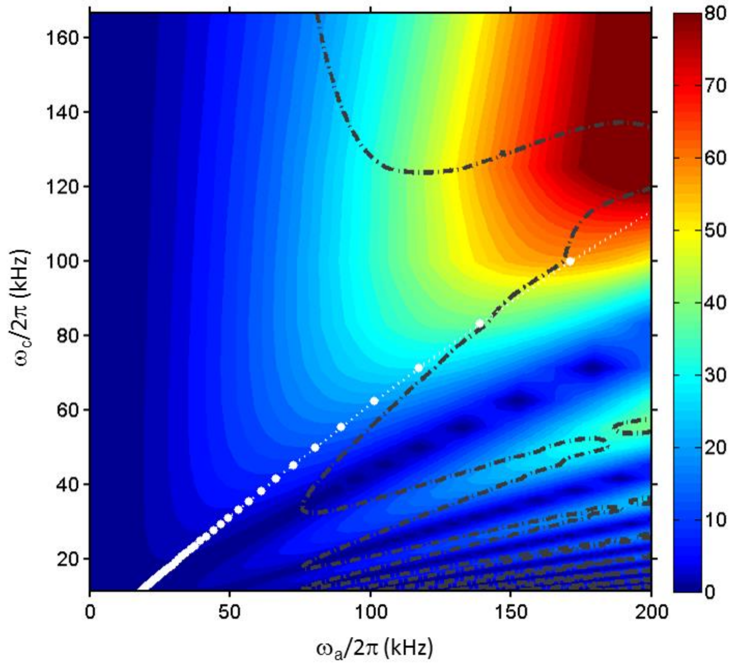

Figure 7 The absolute magnitude (in kHz) of the effective field calculated as in Eq. 9. The calculation was performed for a single spin as a function of its CSA (ω$_a$) and the CPMG periodicity ω$_c$, limiting the Floquet Hamiltonian to k=50 (no powder averaging was considered). In the region to the left of the dashed grey contour, 90% of the effective field points in the y direction . The dotted white line was calculated for $|\omega_a d^{(1)}_{0,1}| = \omega_c$, and above it the van-Vleck transformation is a good approximation for the effective Hamiltonian.

pulses) and its magnitude, which depends on the magnitude of the e-n couplings, can result in an effective spin lock of the magnetization following an excitation pulse in the x direction. Furthermore, this field can partially truncate the residual dipolar interaction in $H^{(0)}$ and in $H^{(1)}$ which would slow the signal's decay as observed in the simulations.

This effect becomes more significant as the CSA interaction increases, however when the off diagonal elements in the original Floquet Hamiltonian (Eq. 6) satisfy $|\omega_a G_a d^{(1)}_{m,k}| \gg k\omega_c$, the van-Vleck diagonalization is no longer a good approximation and we have to evaluate the effect of these large off diagonal terms. To do so, and calculate the effective field formed from the CSA terms for different values of ω_c, we perform an exact diagonalization of the Floquet Hamiltonian (excluding the homonuclear part):

$$\Lambda_F = D_F^{-1}\left\{\sum_k H_k F_k + \omega_c N\right\} D_F = \Lambda_0 F_0 + \omega_c N \qquad (9)$$

The difference between the eigenvalues closest to zero in the diagonalized Hamiltonian, Λ_0, provides the magnitude of the effective field created by the CSA interaction and the diagonalization matrix, D_F, can be used to determine its direction. The result of the calculation for a single spin with increasing chemical shift anisotropy (not including powder averaging) is shown in Figure 7. The calculation was performed for various ω_c values by changing the CPMG inter-pulse delay (and keeping the pulse length fixed). The colour contours represent the total magnitude of the field created by the CSA interaction. To the left of the dashed grey contour 90% of the effective field is in the y direction. The dashed white line marks the region where the largest off diagonal elements satisfy $|\omega_a d^{(1)}_{0,\pm1}| < \omega_c$, and below this line the van-Vleck transformation is not a good enough approximation for the effective Hamiltonian. Thus, overall the effective field points mostly in the y direction, with increasing magnitude when both the CSA and ω_c increase.

However, in the bottom right corner, as the CSA increases and for longer CPMG cycles (low ω_c), regions where the effective field is approaching zero are formed as a result of the increase in the off-diagonal terms with respect to ω_c. In this region, corresponding to a long inter-pulse delay (compared with the magnitude of the spin interactions), the eigenvalues oscillate depending on the difference between ω_c and $|\omega_a G_a d^{(1)}_{0,\pm1}|$, resulting in narrow areas where the effective field crosses zero. An analytical expression for this regime was given by Walls et al.[21] These zero crossings depend on the timings of the CPMG sequence and the CSA interaction and in a powder sample their exact position will depend on the orientations of the crystallites. When these conditions are met, for a fixed ω_c and for specific crystal orientations, they will result in signal decay by the homonuclear interaction which is no longer truncated by the CSA effective field. Thus we can expect that for a broad powder pattern, acquisition with CPMG will result in anisotropic performance across the static line shape, with lower signal for orientations which fall within regions where the effective field approaches zero. This effect can be seen in the experimental spectra in Figure 8a, acquired by Fourier transformation of the signal remaining following a train of CPMG pulses with various ω_c values (by varying the inter-pulse delay τ). The spectra were acquired following a varying number, n, of CPMG pulses which, along with the varying inter-pulse delays, results in different T_2 decays and variation in the spectral quality. Nevertheless the powder pattern reflects the orientation dependent performance of the CPMG sequence which can be qualitatively reproduced by simulations of a small spin system (Figure 8b).

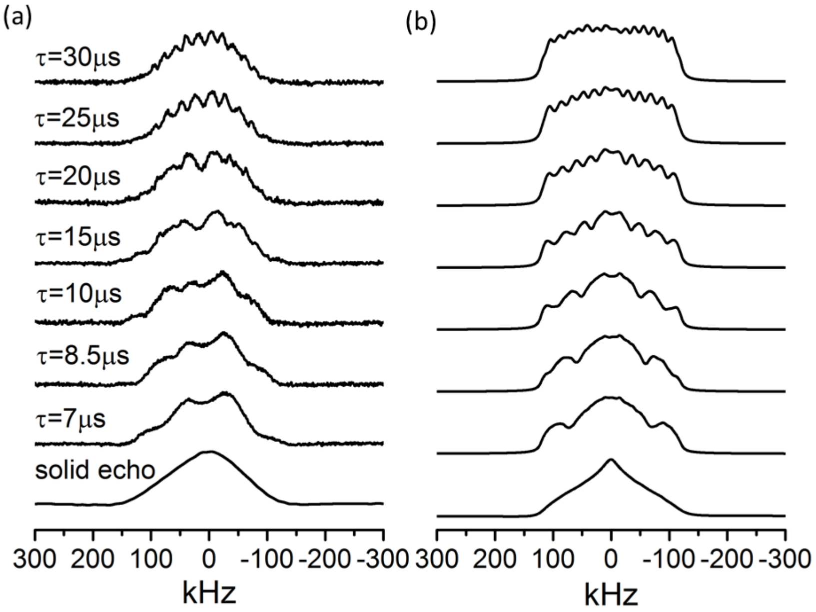

Figure 8 (a) The ^{7}Li static line shape obtained after several blocks of CPMG were applied with varying inter-pulse delay τ as specified on the LHS. The bottom spectrum was obtained with the solid echo sequence (π/2–τ–π/2–τ) for τ=10 μs. (b) Simulated spectra calculated after 50 blocks of CPMG with varying inter-pulse delay and RF amplitude equal to 167 kHz for a system of 6 spins with average homonuclear dipolar couplings of 400 Hz and CSA of 120 kHz (for all spins). Powder averaging was obtained using the ZCW set[40] with 987 orientations and a line broadening of 10 kHz was applied.

4. Conclusions

The application of the CPMG pulse sequence to materials with large anisotropic interactions results in extended signal lifetime as compared with Hahn echo measurements, even when dynamic processes are negligible. Significant signal retention is observed beyond 1 ms for static paramagnetic samples. This effect is due to finite pulse lengths and the presence of large interactions resulting in an effective field which can lock the magnetization during the CPMG pulse train. This effective field partially truncates the homonuclear interactions thereby slowing the signal's decay. For very large interactions this spin-lock effect becomes anisotropic, depending on the exact shape of the static powder pattern and the experimental parameters, resulting in distortions of the powder line shape.

Our results indicate that CPMG decay curves must be interpreted with caution for materials subjected to large anisotropy, often the case in in-situ NMR of paramagnetic electrodes as well as measurements of large static patterns[38] in the presence of homonuclear dipolar couplings. Decay rates obtained with CPMG should not be interpreted simply as transverse relaxation as they are a result of both relaxation and a coherent effect of the spin interactions and RF pulses. Similarly these effects should be taken into account in the application of the CPMG sequence for probing dynamic processes. We note that our experiments and theoretical analysis are limited to the use of high RF amplitudes, higher than or of the order of the anisotropic interactions in the samples studied here. The limit of low RF fields and smaller flip angles, typically employed when CPMG is used for sensitivity enhancement in measurements of static NMR patterns[36,39], was not considered here and may result in different performance.

The extended decay curves observed here with CPMG may be beneficial for applications such as static heteronuclear recoupling in paramagnetic materials. Finally, this study highlights the importance of developing a deeper understanding of the effects of the dominant paramagnetic interactions during multiple pulse experiments so as to extend the experimental arsenal available for static and in-situ investigations of paramagnetic materials.

Acknowledgments

We thank Dr. Frederick Omenya for providing the samples and Hao Liu for the ^{6,7}LiFePO$_4$ spectra. We are grateful to Prof. Shimon Vega, Dr. Gonzalo A. Alvarez and Dr. Lina Zhou for insightful discussions. We acknowledge support provided by the Assistant Secretary for Energy Efficiency and Renewable Energy, Office of Vehicle Technologies of the U.S. DOE, under Contract DE-AC02-05CH11231, as part of the BATT Program; Subcontract 6517749.

References

(1) Pintacuda, G.; Kervern, G. In *Modern NMR Methodology SE - 312*; Heise, H.; Matthews, S., Eds.; Topics in Current Chemistry; Springer Berlin Heidelberg: Berlin, Heidelberg, 2012; Vol. 335, pp. 157–200.

(2) Grey, C. P.; Dupré, N. *Chem. Rev.* **2004**, *104*, 4493–4512.

(3) Strobridge, F. C.; Middlemiss, D. S.; Pell, A. J.; Leskes, M.; Clément, R. J.; Pourpoint, F.; Lu, Z.; Hanna, J. V.; Pintacuda, G.; Emsley, L.; Samoson, A.; Grey, C. P. *J. Mater. Chem. A* **2014**, *2*, 11948–11957.

(4) Hung, I.; Zhou, L.; Pourpoint, F.; Grey, C. P.; Gan, Z. *J. Am. Chem. Soc.* **2012**, *134*, 1898–1901.

(5) Clément, R. J.; Pell, A. J.; Middlemiss, D. S.; Strobridge, F. C.; Miller, J. K.; Whittingham, M. S.; Emsley, L.; Grey, C. P.; Pintacuda, G. *J. Am. Chem. Soc.* **2012**, *134*, 17178–17185.

(6) Blanc, F.; Leskes, M.; Grey, C. P. *Acc. Chem. Res.* **2013**, *46*, 1952–1963.

(7) Zhou, L.; Leskes, M.; Ilott, A. J.; Trease, N. M.; Grey, C. P. *J. Magn. Reson.* **2013**, *234*, 44–57.

(8) Zhou L.; Leskes M.; Grey C.P. *unpublished results*.

(9) Carr, H.; Purcell, E. *Phys. Rev.* **1954**, *94*, 630–638.

(10) Meiboom, S.; Gill, D. *Rev. Sci. Instrum.* **1958**, *29*, 688–691.

(11) Álvarez, G. A.; Suter, D. *Phys. Rev. Lett.* **2011**, *107*, 1–5.

(12) Tollinger, M.; Skrynnikov, N. R.; Mulder, F. A. A.; Forman-Kay, J. D.; Kay, L. E. *J. Am. Chem. Soc.* **2001**, *123*, 11341–11352.

(13) Smith, P. E. S.; Bensky, G.; Alvarez, G. A.; Kurizki, G.; Frydman, L. *Proc. Natl. Acad. Sci.* **2012**, *109*, 5958–5961.

(14) Álvarez, G. A.; Shemesh, N.; Frydman, L. *J. Chem. Phys.* **2014**, *140*, 84205–84213.

(15) Leskes, M.; Madhu, P. K.; Vega, S. *Prog. Nucl. Magn. Reson. Spectrosc.* **2010**, *57*, 345–380.

(16) Dementyev, A. E.; Li, D.; MacLean, K.; Barrett, S. E. *Phys. Rev. B* **2003**, *68*, 153302–153306.

(17) Li, D.; Dong, Y.; Ramos, R.; Murray, J.; MacLean, K.; Dementyev, A.; Barrett, S. *Phys. Rev. B* **2008**, *77*, 214306–214334.

(18) Franzoni, M. B.; Levstein, P. R.; Raya, J.; Hirschinger, J. *Phys. Rev. B - Condens. Matter Mater. Phys.* **2008**, *78*, 1–5.

(19) Li, D.; Dementyev, A.; Dong, Y.; Ramos, R.; Barrett, S. *Phys. Rev. Lett.* **2007**, *98*, 190401–190405.

(20) Franzoni, M. B.; Acosta, R. H.; Pastawski, H. M.; Levstein, P. R. *Philos. Trans. R. Soc. A Math. Phys. Eng. Sci.* **2012**, *370*, 4713–4733.

(21) Ridge, C. D.; O'Donnell, L. F.; Walls, J. D. *Phys. Rev. B - Condens. Matter Mater. Phys.* **2014**, *89*, 024404–024422.

(22) Omenya, F.; Wen, B.; Fang, J.; Zhang, R.; Wang, Q.; Chernova, N. a.; Schneider-Haefner, J.; Cosandey, F.; Whittingham, M. S. *Adv. Energy Mater.* **2015**, *5*, 1401204–1401213.

(23) Chen, J.; Vacchio, M. J.; Wang, S.; Chernova, N.; Zavalij, P. Y.; Whittingham, M. S. *Solid State Ionics* **2008**, *178*, 1676–1693.

(24) Chen, G.; Shukla, A. K.; Song, X.; Richardson, T. J. *J. Mater. Chem.* **2011**, *21*, 10126–10133.

(25) Nayeem, A.; Yesinowski, J. P. *J. Chem. Phys.* **1988**, *89*, 4600–4608.

(26) Lee, Y. J.; Grey, C. P. *J. Phys. Chem. B* **2002**, *106*, 3576–3582.

(27) Clément R. J.; Grey, C. P. *unpublished results*.

(28) Middlemiss, D. S.; Ilott, A. J.; Clément, R. J.; Strobridge, F. C.; Grey, C. P. *Chem. Mater.* **2013**, *25*, 1723–1734.

(29) De Paëpe, G.; Giraud, N.; Lesage, A.; Hodgkinson, P.; Böckmann, A.; Emsley, L. *J. Am. Chem. Soc.* **2003**, *125*, 13938–13939.

(30) Drain, L. E. *Proc. Phys. Soc.* **1962**, *80*, 1380–1382.

(31) Schwerk, U.; Michel, D.; Pruski, M. *J. Magn. Reson. Ser. A* **1996**, *119*, 157–164.

(32) Kubo, A.; Spaniol, T.; Terao, T. *J. Magn. Reson.* **1998**, *133*, 330–340.

(33) Veshtort, M.; Griffin, R. G. *J. Magn. Reson.* **2006**, *178*, 248–282.

(34) Balibanu, F.; Hailu, K.; Eymael, R.; Demco, D. E.; Blümich, B. *J. Magn. Reson.* **2000**, *145*, 246–258.

(35) Larsen, F. H.; Jakobsen, H. J.; Ellis, P. D.; Nielsen, N. C. *J. Magn. Reson.* **1998**, *131*, 144–147.

(36) Hung, I.; Gan, Z. *J. Magn. Reson.* **2010**, *204*, 256–265.

(37) Leskes, M.; Akbey, Ü.; Oschkinat, H.; Van Rossum, B. J.; Vega, S. *J. Magn. Reson.* **2011**, *209*, 207–219.

(38) Schurko, R. W. *Acc. Chem. Res.* **2013**, *46*, 1985–1995.

(39) Medek, A.; Frydman, V.; Frydman, L. *J. Phys. Chem.* **1999**, 4830–4835.

(40) Zaremba, S. K. *Ann. di Mat. Pura ed Appl. Ser. 4* **1966**, *73*, 293–317.